Neuro-Oncology Practice
7(6), 646–655, 2020 | doi:10.1093/nop/npaa047 | Advance Access date 15 August 2020

Multiparameter quantitative histological MRI values in high-grade gliomas: a potential biomarker of tumor progression

Gilles Reuter, Emilie Lommers, Evelyne Balteau, Jessica Simon, Christophe Phillips, Felix Scholtes, Didier Martin, Arnaud Lombard, and Pierre Maquet

GIGA Cyclotron Research Centre–In Vivo Imaging, University of Liège, Liège, Belgium (G.R., E.L., E.B., C.P., P.M.); Department of Neurosurgery, University Hospital of Liège, Liège, Belgium (G.R., F.S., D.M., A.L.); Department of Neurology, University Hospital of Liège, Liège, Belgium (E.L., P.M.); Psychology and Neuroscience of Cognition–PsyNCogn, University of Liège, Liège, Belgium (J.S.); GIGA In Silico Medicine, University of Liège, Liège, Belgium (C.P.); Laboratory of Developmental Neurobiology, GIGA–Neurosciences Research Center, University of Liège, Liège, Belgium (F.S., A.L.); and Department of Neuroanatomy, University of Liège, Liège, Belgium (F.S.)

Corresponding Author: Gilles Reuter, MD, Neurosurgery, Centre Hospitalier Universitaire (CHU) de Liège, Bat B35, Domaine Universitaire du Sart-Tilman, 4000, Liège, Belgium (gilles.reuter@chuliege.be).

Abstract

Background. Conventional MRI poorly distinguishes brain parenchyma microscopically invaded by high-grade gliomas (HGGs) from the normal brain. By contrast, quantitative histological MRI (hMRI) measures brain microstructure in terms of physical MR parameters influenced by histochemical tissue composition. We aimed to determine the relationship between hMRI parameters in the area surrounding the surgical cavity and the presence of HGG recurrence.

Methods. Patients were scanned after surgery with an hMRI multiparameter protocol that allowed for estimations of longitudinal relaxation rate (R1) = 1/T1, effective transverse relaxation rate (R2)*=1/T2*, magnetization transfer saturation (MT_{sat}), and proton density. The initial perioperative zone (IPZ) was segmented on the postoperative MRI. Once recurrence appeared on conventional MRI, the area of relapsing disease was delineated (extension zone, EZ). Conventional MRI showing recurrence and hMRI were coregistered, allowing for the extraction of parameters R1, R2*, MT_{sat}, and PD in 3 areas: the overlap area between the IPZ and EZ (OZ), the peritumoral brain zone, PBZ (PBZ = IPZ – OZ), and the area of recurrence (RZ = EZ – OZ).

Results. Thirty-one patients with HGG who underwent gross-total resection were enrolled. MT_{sat} and R1 were the most strongly associated with tumor progression. MT_{sat} was significantly lower in the OZ and RZ, compared to PBZ. R1 was significantly lower in RZ compared to PBZ. PD was significantly higher in OZ compared to PBZ, and R2* was higher in OZ compared to PBZ or RZ. These changes were detected 4 to 120 weeks before recurrence recognition on conventional MRI.

Conclusions. HGG recurrence was associated with hMRI parameters' variation after initial surgery, weeks to months before overt recurrence.

Keywords

high-grade gliomas | quantitative magnetic resonance imaging | peritumoral brain zone | tumor progression

High-grade gliomas (HGGs) are both the most common and most malignant primary brain tumors. Despite major advances in their treatment and follow-up, the prognosis remains poor because of systematic recurrences.[1] In addition to age, risk factors include male sex, previous ionizing radiation, white ethnicity, and rare genetic diseases.[2] The development of glioma is also positively correlated with brain size, suggesting that it arises from a stochastic event related to the number of cells at risk. When adjusted for brain size, the risk of glioma is slightly higher for females.[3]

The reasons for treatment failure are manifold. First, the detection of an HGG comes relatively late in the course of its development, either because of its progression from a previous lower-grade glioma or to the late outbreak of symptoms. However, population-based screening has proven neither beneficial nor cost-effective, stressing the need for noninvasive methods of early detection.[4] Second, on postmortem examinations, malignant cells can be identified far away from the tumor by conventional MRI.[5,6] Therefore, even when surgery removes all contrast-enhancing brain tissue and surrounding fluid-attenuated inversion recovery (FLAIR) abnormality,[7,8] viable tumor cells remain in the brain. Various techniques were developed to alleviate this caveat, to date having some effect on outcome: neuro-navigation,[9] fluorescence-guided surgery using 5-aminolevulinic acid,[10] intraoperative MRI, and Raman spectroscopy.[11] Third, different radiotherapy regimens are recommended but do not significantly modify the outcome.[12–14] Finally, the cognitive side effects of brain irradiation seem to be dose related.[15,16]

Thus, novel techniques more sensitive to the presence of tumoral tissue than conventional MRI are urgently needed. Unfortunately, despite the abundance of novel imaging techniques (MR perfusion techniques and analyses of regional cerebral blood volume,[17–19] S-transform–based texture analysis of T1-weighted (T1w) and T2-weighted (T2w) images,[20] MR spectroscopy,[21] apparent diffusion coefficient,[22] chemical exchange saturation transfer,[23] dynamic contrast-enhanced MRI,[24] diffusion tensor imaging[25]), no MR biomarker has so far been able to robustly and accurately predict the localization of HGG recurrence.

Although in vivo brain MRI cannot directly image neurons or glial cells, the combination of advanced quantitative MRI with biophysical models of MR contrast allows one to make inferences about the brain microscopic structure, thereby approaching in vivo histology MRI (hMRI). hMRI has pushed accessible image resolutions into the "mesoscopic scale" (0.1 mm-0.5 mm), which comprises between macroscopic and microscopic scale, enabling in vivo imaging of features including cortical laminae, cortical columns, dural lymphatic vessels, and vasculature.[26]

hMRI harnesses the advantages of quantitative MRI methods that measure physical tissue parameters such as the longitudinal relaxation rate (R1 = 1/T1), the effective transverse relaxation rate (R2* = 1/T2*), the magnetization transfer saturation (MT_{sat}), and proton density (PD).[26] R1 is sensitive to interactions of water molecules with other water molecules, water molecules bound to macromolecules, and the paramagnetic centers found in cortical tissue. R2* is strongly sensitive to paramagnetic iron. The MT signal arises from the exchange between fast relaxing water bound to macromolecules and slowly relaxing unbound water molecules. In consequence, MT_{sat} depends strongly on the tissue macromolecular content. PD measures the free water content of a voxel and decreases with the density of MR-invisible macromolecules (eg, lipids and proteins).[27] Because hMRI is quantitative, the measures of physical MR parameters are more reproducible across participants and scanners than weighted MRI.[28] Currently, hMRI has been used to track age-related changes in brain microstructure,[29] posttraumatic degeneration,[30] and alterations in normal-appearing gray and white matter of patients with multiple sclerosis,[31] Alzheimer disease, microangiopathy, and paraneoplastic disease.[32]

Here we capitalized on its high sensitivity to variations in brain tissue microstructure to assess, in the postoperative period, whether quantified MR parameters in the peritumoral brain zone (PBZ) differed between the regions of HGG recurrence and the regions without evidence of tumor recurrence.

Methods

The local ethics committee approved this prospective observational study (B707201316912). Written informed consent was obtained from each patient before inclusion. Data acquisition ran from September 2013 to December 2017.

Population

In a single neurosurgical department, all patients with histological diagnosis of HGG (anaplastic astrocytoma [AA], anaplastic oligodendroglioma [AO], and glioblastoma [GBM]) and gross total resection (GTR) based on immediate postoperative MRI showing no residual enhancing tissue were eligible. Exclusion criteria were age younger than 18 years, postoperative KPS less than 50, World Health Organization performance status greater than 3, contraindications to MRI. All patients were discussed in multidisciplinary neuro-oncology meetings and treated according to European Association for Neuro-Oncology (EANO) guidelines.[12]

Data Acquisition

Patients were asked to participate in the study once the diagnosis of HGG was histologically confirmed after surgery. Each patient had standard follow-up MRI every 3 months. This included T2w, FLAIR, diffusion-weighted imaging, and multiplanar 1 mm T1w pregadolinium (pre-Gd) and post-Gd contrast-enhanced sequences (Magnetom Symphony 1.5T, Magnetom Aera 1.5T, Magnetom Vida 3T Siemens Medical Solutions).

A single experimental MRI session was scheduled at least 8 weeks (maximum 36 weeks) after surgery to minimize the risks of postoperative artifacts.[33] Multiparameter quantitative histological MRI (MP-hMRI) data were acquired on a 3T head-only MRI-scanner (Magnetom Allegra, Siemens Medical Solutions) or on a 3T whole-body MRI-scanner (Magnetom Prisma, Siemens Medical Solutions). The whole-brain MRI acquisitions included

a multiparameter mapping protocol, developed in the framework of an international collaborative effort including several sites.[29,34,35] This protocol consists of 3 colocalized 3-dimensional multiecho fast low angle shot (FLASH) acquisitions at $1 \times 1 \times 1$ mm^3 resolution and 2 additional calibration sequences (B1+, B1–) to correct for inhomogeneities in the radiofrequency (RF) transmit field. The FLASH data sets were acquired with predominantly PD, T1, and MT weighting. All 3 had high bandwidth to minimize off-resonance and chemical shift artifacts. Volumes were acquired in 176 sagittal slices using a 256 × 224-voxel matrix. GRAPPA parallel imaging was combined with partial Fourier acquisition to speed up acquisition time in approximately 20 minutes.

MRI Images Processing

We used SPM 12 (www.fil.ion.ucl.ac.uk/spm) and an additional SPM toolbox: (http://hmri.info/) in Matlab (Matlab R2015b, The MathWorks Inc) to process the data. Quantitative maps were computed from native images using the hMRIToolbox, generating maps of MT_{sat}, effective transverse relaxation rate (R2*), longitudinal relaxation rate (R1) and PD* maps.[36] Briefly, echoes for T1w, PDw, and MTw were extrapolated to echo time (TE) = 0 to increase the signal-to-noise ratio and suppress the R2* bias.[37,38] The resulting MTw and T1w (TE = 0) images were used to calculate MT_{sat} and R1 maps. Quantitative R1 and MT_{sat} maps were corrected for local RF transmit field inhomogeneity and imperfect RF spoiling with the 2 aforementioned (B1+, B1–) calibration sequences.[39,40] MT_{sat} measures the percentage loss of magnetization resulting from the MT prepulse used. MT_{sat} differs from the commonly used MT ratio (MTR) by explicitly accounting for spatially varying T1 relaxation time and flip angles. The MT_{sat} map shows a better contrast-to-noise ratio than the MTR.[41] Quantitative R2* was estimated from all 3 multiecho series (PDw, MTw, and T1w) using the ESTATICS model.[37]

Based on the T1w maps acquired in the MP-hMRI protocol, we manually delineated a region of interest (ROI) of brain tissue with abnormal appearance on T1 and R2* images around the surgical cavity called the initial perioperative zone (IPZ). This ROI is presumably composed of brain parenchyma, edema, and tumor infiltration and corresponds to FLAIR abnormality around the cavity.[13]

Based on the first follow-up clinical MRI that showed tumor progression on T1 + Gd, we manually delineated a second ROI that corresponded to the contrast-enhancing signal of the recurrent disease (extension zone, EZ). Patients who could be reoperated on and in whom recurrence was histologically confirmed (ruling out pseudoprogression or radionecrosis) were also included in the study. The delineation of abnormal-appearing brain parenchyma and ROIs was performed by a senior neurosurgeon with more than 10 years' experience in neurosurgery (G.R.) and double-checked by a senior neurologist with more than 30 years' experience in computational neuroimaging (P.M.).

The 4 parametric maps (MT_{sat}, R1, R2*, and PD), the 3-dimensional-T1Gd (recurrence MRI), and the corresponding ROIs were coregistered using a rigid-body transform and normalized mutual information approach.[42] From these, we identified the area of overlap (overlap zone, OZ) between the IPZ and EZ. We also defined the recurrence zone (RZ; ie, EZ – OZ). The PBZ was defined as a FLAIR abnormality without evidence of tumor recurrence (PBZ = IPZ – EZ) (Figure 1).

Voxel values of MT_{sat}, R1, R2*, and PD were extracted from the corresponding coregistered parametric map in PBZ and RZ (see Figure 1). From these, we computed the mean voxel values in the area of overlap between the 2 ROIs (OZ), as well as the mean value of the initial PBZ and RZ (this time after exclusion of their overlap). This system provided 3 areas of interest (initial PBZ, RZ, and OZ) and 4 tissue parameters (MT_{sat}, R1, R2*, and PD) in the ipsilateral part of the brain. Statistical analyses were all performed using Jamovi software (The jamovi project [2019]. *jamovi*. [version 1.1.9] [computer software]; https://www.jamovi.org). First, we proceeded to a mixed analysis of variance (ANOVA) with ROIs (PBZ vs RZ vs OZ) as repeated measures and the scanner as between-subject variable on the median value of each parameter. In case of sphericity violation identified by the Mauchly test, we applied the Greenhouse-Geisser correction. Partial eta squared (η) was used as a measure of effect size. In case of significant main effect or interaction, we performed the Tukey honestly significant difference post hoc test to account for multiple comparisons across 3 areas (peritumoral vs overlap, overlap vs recurrence, peritumoral vs recurrence), see Supplementary material. Second, we compared the median value between the abnormal-appearing white matter ROI and the recurrence ROI for each parameter using a mixed ANOVA with ROIs (PBZ vs RZ) as repeated measures and the scanner as between-subject variable to include patients in whom recurrence was not located in the abnormal-appearing white matter ROI (n = 3). To confirm the equivalence between both scanners, we performed a 2 one-sided equivalence test (TOST). Finally, multiple linear regression analyses were conducted to explain progression-free (PFS) and overall survival by the 4 tissue parameters (MT_{sat}, R1, R2*, and PD) in the PBZ and RZ areas.

Results

Demographics

Thirty-one patients were included in the study. Two patients who had interrupted MRI follow-up or died before follow-up showed recurrent contrast enhancement. Among the 29 patients who showed recurrent contrast enhancement suggesting HGG recurrence, 22 showed clinical and radiological progression despite steroid administration. In 7 patients, pseudoprogression or radionecrosis were diagnosed, based on diffusion imaging, perfusion imaging, and [^{18}F]-fluoro-deoxyglucose PET criteria.[43] Among the 22 patients who showed clear recurrence, we found an overlap between the IPZ ROI and the recurrence ROI in 19 cases. In 3 cases, recurrence was located outside this area. The delays between the initial resection and the MP-hMRI acquisition ranged from 8 to 36 weeks (median, 14 weeks).

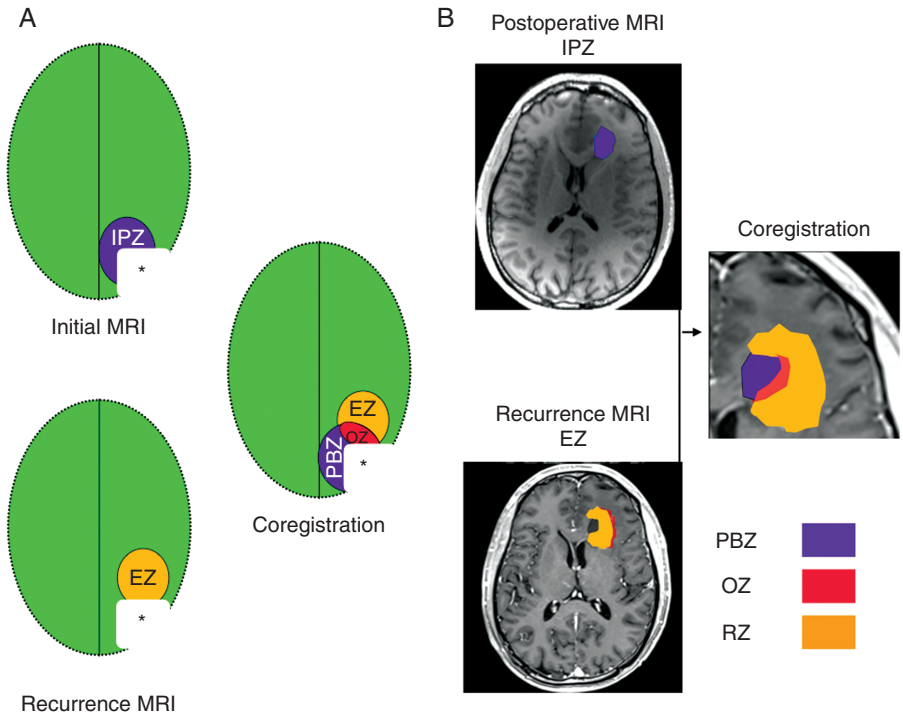

Figure 1. Diagram of the different coregistered regions of interest. A, *Corresponds to the surgical cavity. Initial perioperative zone (IPZ) corresponds to initial postoperative fluid-attenuated inversion recovery (FLAIR) abnormality. Extension zone (EZ) corresponds to later gadolinium-enhanced progression. Overlap zone (OZ) is the overlap between IPZ and EZ. Recurrence zone (RZ) corresponds to gadolinium-enhanced progression outside the initial FLAIR abnormality (RZ = EZ-OZ). Peritumoral brain zone (PBZ) corresponds to the initial FLAIR abnormality outside the EZ. (PBZ = IPZ – EZ). B, Postoperative histological MRI (hMRI) and follow-up conventional T1-weighted MRI + gadolinium are automatically coregistered with SPM 12, thereby defining PBZ, OZ, and RZ.

From initial resection to the MP-hMRI, all patients received radiation therapy. A small variation in radiation regimen must be mentioned: 60 Gy in 30 fractions was delivered for GBM, and a dose of 59.4 Gy in 33 fractions was given for AAs and AOs. GBM patients received concomitant temozolomide during that phase.

After MP-hMRI, all patients followed adjuvant treatment according to EANO guidelines.[12] GBM and AA patients received temozolomide after irradiation and AO patients received PCV (procarbazine, lomustine, and vincristine) after irradiation.

The MP-hMRI was acquired during the adjuvant treatment phase, during the time window between concomitant radiochemotherapy and chemotherapy alone. We considered that early postoperative changes could flaw data from the peritumoral zone during the first postoperative weeks. Indeed, diffusion studies reported that values were modified in the peritumoral zone right after surgery.[44,45] Likewise, radiation therapy also can induce posttreatment modifications although they typically occur several weeks to months after the end of irradiation.[46]

The outlier patient for whom acquisition was delayed (36 weeks) was a patient who was misdiagnosed with low-grade glioma and then reclassified as isocitrate dehydrogenase wild-type GBM (IDH_{WT}-GBM) and was therefore offered adjuvant therapy.

The delay between the initial MP-hMRI acquisition and the follow-up MRI showing a recurrence ranged from 4 to 120 weeks (median, 36 weeks). After surgery, each patient had a standard follow-up MRI every 3 months or earlier in case of clinical deterioration as recommended by EANO guidelines.[47] For the comparison between MP-hMRI and follow-up MRI, we considered only the first follow-up MRI that showed clear recurrence. This time frame of 4 to 120 weeks between MP-hMRI and recurrence MRI corresponds to a PFS of 12 to 156 weeks, which is in line with current literature results for a sample of 22 GBMs, 5 AAs, and 4 AOs.[48,49]

Histology at inclusion was AA (n = 5), AO (n = 4), and GBM (n = 22). Mean PFS was 52 weeks (range, 12-156 weeks) (Figure 2;Table 1 and Supplementary material).

Statistical Results

The mixed ANOVAs showed a main effect of the ROIs on each parameter (for MT_{sat}: [F(2,34) = 8.76, $P < .001$, =0.34], for PD: [F(2,34) = 4.20, $P = .02$, =0.20], for R1: [F(2,34) = 7.68, $P = .002$, =0.31], and for R2*: [F(1.51,25.70) = 4.84, $P = .02$, =0.22)] (Figures 3 and 4). The post hoc test revealed a higher mean value of MT_{sat} parameter in the PBZ compared to the OZ ($P = .03$) and the RZ ($P < .001$), and the RZ and OZ did not differ from each other ($P = .31$). The mean

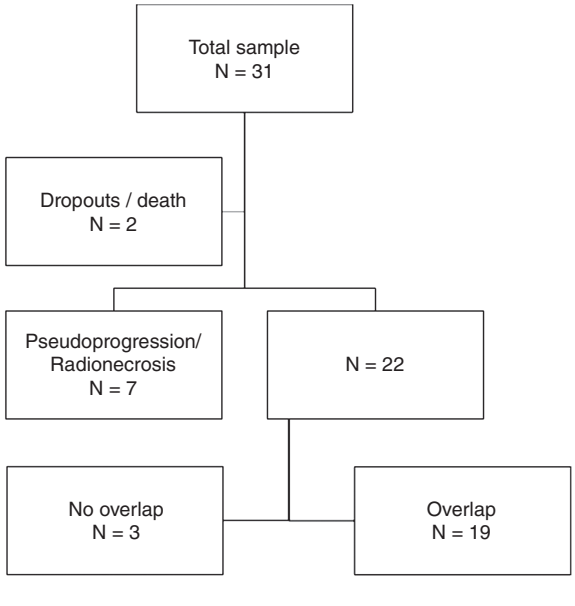

Figure 2. Population Samples.

value of the PD parameter is lower in the PBZ than in the OZ ($P = .03$), whereas there was no significant difference between the other comparisons (PBZ vs RZ: $P = .07$, RZ vs OZ, $P = .92$). The mean value of the R1 parameter is higher in the PBZ than in the RZ ($P = .001$), whereas there was no difference between the other comparisons (PBZ vs OZ: $P = .23$, RZ vs OZ, $P = .08$). Finally, the mean value of the R2* parameter is higher in the OZ compared to the PBZ ($P = .05$) and RZ ($P = .02$), which did not differ from each other ($P = .90$). We found no significant main effect of the scanner (Magnetom Allegra vs Magnetom Prisma, all $P > .16$) nor an interaction between the scanner and repeated measures (all $P > .09$).

We also performed a mixed ANOVA including the patients for whom the recurrence was located away from the abnormal-appearing white matter, with no contact with the vicinity of the surgical cavity. MT_{sat} ($F[1,20] = 9.49$, $P = .006$, $=0.32$) and R1 ($F[1,20] = 7.49$, $P = .01$, $=0.27$) parameters were again significantly lower in the RZ than in the PBZ, whereas the difference was not significant for the other parameters (for PD: $F[1,20] = 2.76$, $P = .11$, $=0.12$, R2*: $F[1,20] = 0.18$, $P = .68$, $=0.01$). We found no significant main effect of the scanner (all $P > .16$) nor a interaction between the scanner and repeated measures (all $P > .19$).

We conducted a TOST equivalence test for each parameter to compare scanner 1 vs scanner 2 data (see Supplementary material). This test showed no statistical difference between both scanners for all parameters (MT $P = .474$, R1 $P = .693$, R2* $P = .450$, PD $P = .145$) and showed equivalence for all parameters for both scanners (MT: $P_{Upper} = .029$, $P_{Lower} = .002$, R1: $P_{Upper} = .007$, $P_{Lower} = .002$, R2* $P_{Upper} = .002$, $P_{Lower} = .047$, PD $P_{Upper} = .050$, and $P_{Lower} < .001$.

Finally, the parameter in the PBZ and RZ did not statistically explain PFS ($F[8,13] = 0.45$, $P = .87$, $R^2 = 0.22$) nor OS ($F[8,13] = 1.27$, $P = .34$, $R^2 = 0.44$).

Table 1. Study Population Data n = 29 (Study Dropouts Excluded)

Age, y	**Min 17, max 75, median 52.5, mean 49.34**
Sex	Female n = 6, male n = 23
Diagnosis at inclusion	Anaplastic astrocytoma n = 5 (17.2%), anaplastic oligodendroglioma n = 4 (13.8%), glioblastoma n = 22 (75.9%)
Epilepsy during follow-up	n = 14 (48%)
Motor deficit at diagnosis	n = 8 (27.5%)
Maximal size in T1 + Gd at diagnosis, mm	Min 0, max 80.6, mean 41.03, median 40
Maximal size in T2 at diagnosis, mm	Min 20.7, max 126, mean 67.9, median 70
Location	Frontal n = 12 (41.3%), temporal n = 8 (27.5%), temporoparietal n = 2 (6.8%), occipital n = 1 (3.4%), central n = 4 (13.8%), insular n = 2 (6.8%)
Ki67 (%)	Min 3, max 70, mean 24.8, median 20
MGMT promoter methylation	n = 16 (55%)
IDH-1 mutation	Negative n = 15 (51.7%), positive n = 9 (31%), unknown n = 3 (10.3%)
Operative complications	1 meningitis, 2 intratumoral bleedings

Abbreviations: Gd, gadolinium; *IDH-1*, isocitrate dehydrogenase 1; max, maximum; *MGMT*, O6-methylguanine–DNA methyltransferase; Min, minimum.

Discussion

The main result of this prospective study is that quantitative MR parameters differ within the initial perioperative area between the region where HGG will subsequently recur (OZ and RZ) and the area where it will not (PBZ). These differences in brain microstructure, characterized by a decrease in MT_{sat} and an increase PD in OZ and a sharper fall of MT_{sat} and R1 in RZ, antedate by weeks the recurrence visible on conventional MRI. This suggests that they result from microstructural modifications induced by infiltrating tumor tissue, macroscopically undetectable by intraoperative inspection or conventional MRI.

Little is known about the microstructural changes associated with occult tumor invasion. Preoperatively, R1 and R2* decrease with increasing distance from the contrast-enhancing part of the tumor.[50] Within the preoperative peritumoral FLAIR hypersignal, a bimodal pattern of relaxation values suggested a distinction between peritumoral edema (high R1) and nonenhancing infiltrating tumor (low R1).[50] T1 was shown to be prolonged (ie, R1 shortened) before any change was detectable by conventional MR in the peritumoral brain of 6 patients with recurrent GBM under bevacizumab, suggesting tumor progression.[51] Likewise, postoperative

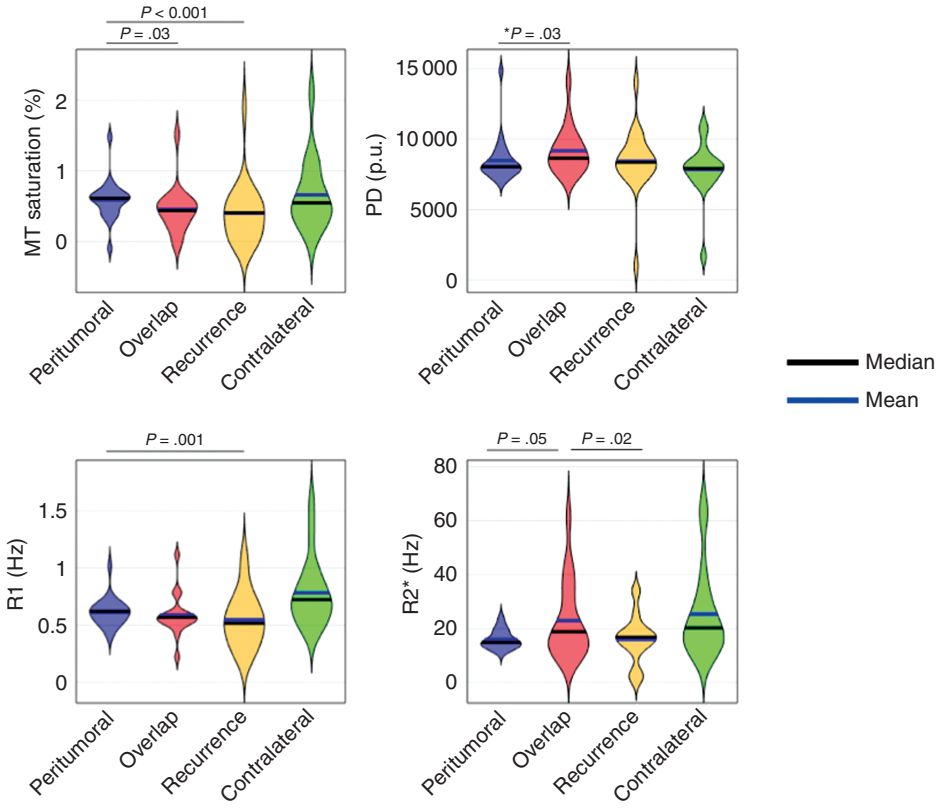

Figure 3. Parameters distribution. Violin diagrams of the parameters in the peritumoral brain zone, overlap zone, recurrence zone, and contralateral hemisphere. Ipsilateral statistically significant differences are displayed for each parameter. MT, magnetization transfer. OZ, overlap zone; PBZ, peritumoral brain zone; R1, longitudinal relaxation rate; RZ, recurrence zone.

	MTsat (*p.u*)	R1 (*Hz*)	R2* (*Hz*)	PD (*p.u*)
Peritumoral brain zone (PBZ) Mean (SD)	0.58 (0.28)	0.61 (0.12)	15.93 (3.42)	8496.4 (1609.53)
Overlap (OZ) Mean (SD)	0.44 (0.32)	0.58 (0.17)	21.88 (14.03)	8873.70 (1654.14)
Recurrence (RZ) Mean (SD)	0.38 (0.41)	0.52 (0.20)	15.58 (8.56)	9131.52 (1576.59)
Contralateral to PBZ Mean (SD)	0.66 (0.40)	0.75 (0.23)	23.22 (10.74)	7811.85 (1610.23)

Figure 4. Mean values and SDs of the quantitative parameters inside each relevant region of interest (ROI). R1, longitudinal relaxation rate; R2, effective transverse relaxation rate.

hMRI in 13 GBMs found that the MTR was lower in the tumor area compared to the contralateral hemisphere.[52] These results agree with the current postoperative findings of lower MT_{sat} and R1 in the area where the HGG will recur (Figure 5).

The histological underpinning of the changes in quantitative parameters remains uncertain. In this study, PD was higher in the OZ compared to the PBZ. Blystad et al[50] also found a bimodal distribution of PD values in a peritumoral edema with high values associated with infiltration and low values associated with edema. Here, we included patients only after surgery, when very little edema is observed. Therefore, we hypothesize that high PD values are correlated with tumor infiltration.

MT_{sat}, a parameter strongly related to myelin content,[53,54] is robustly decreased in the OZ and even more so in the RZ compared to PBZ. During the invasion phase, glioma cells produce matrix metalloproteinases that degrade extracellular matrix (ECM) components and allow remodeling of the ECM around blood vessels or white-matter tracts. It is tempting to suggest that MT_{sat} is correlated to ECM integrity and that glioma extension, inducing ECM destruction, would result in MT_{sat} diminution along the way of glioma progression.

R1, the longitudinal relaxation rate (R1 = 1/T1), is influenced by different factors: water content, iron concentration, and coherence of macromolecules, such as myelin.[55] In this study, R1 was significantly lower in the OZ and RZ compared to the PBZ. R1 was even lower in the RZ than the OZ. ECM contents might be destroyed along the way of glioma invasion and it has also been recently understood that iron avidity is enhanced in HGG because of inflammation.[56,57] R1 decreases as glioma invades brain tissue but may increase as a result of iron avidity in the proliferating/necrotic core. These 2 phenomena therefore act competitively on R1 value. The R1 value will be only slightly affected where ECM is destroyed and necrosis present (low R1 in the OZ) and more affected where ECM is destroyed but necrosis/inflammation is absent (lower R1 in the RZ). By contrast, R1 was significantly lower in the PBZ compared to the contralateral hemisphere, suggesting that the most important modification of the R1 parameter was due to tumor infiltration (low R1) and not edema (high R1). Also, MT and R1 tend to decrease with aging, especially in white matter;[29] we report within-subjects results only, which rules out any age effect.

R2*, the effective transverse relaxation rate (1/T2*), is affected by nonheme iron, mainly found in oligodendrocytes and myelin,[58] but also by myelin content, fiber orientation, and water content. We also found that R2* was lower in the RZ compared to the OZ ($P = .02$); we interpret this result as, in the whole recurrence, a high R2* correlates with an increase in iron content in the most aggressive part of the tumor. Also, R2* was significantly lower in the PBZ than in the contralateral hemisphere. Mehrabian and colleagues have found that in white matter contralateral to the tumor, the T2 signal tends to be higher (lower R2) than in the white matter of healthy controls,[52] suggesting that relaxometric parameters are already modified in a normal-appearing hemisphere. In line with these results, here we found that R2* was lower in the PBZ compared to the contralateral hemisphere.

Finally, MT in the tumor before surgery, inferred from chemical exchange saturation transfer MRI, was found by Regnery et al to be significantly lower in patients with GBM in whom the tumor will progress earlier than in those in whom GBM will progress slowly (ie, stable disease).[23] The authors found a significant relationship between MTR and PFS. This was not the case in the present investigation. The cause of this discrepancy might first be related to the population. In this study, we included grade 3 tumors and GBMs, whereas Regnery and colleagues exclusively included GBMs. Because GBM has a more destructive pattern, we could expect that this difference might partially be

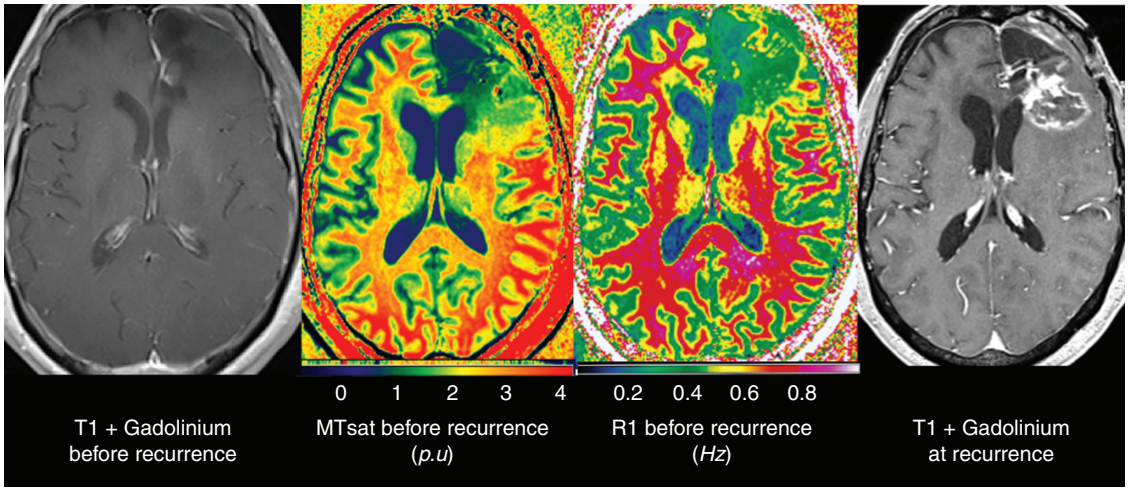

Figure 5. Exemplative case of a patient with glioblastoma before recurrence was noted. T1 + gadolinium on the left; magnetization transfer saturation (MT_{sat}) and longitudinal relaxation rate (R1) were acquired at the same time. MT_{sat} and R1 show a clear decrease where recurrence will appear 5 months later, with T1 + gadolinium on the right.

related to that destructive effect of GBM on MT. Second, Regnery et al predicted PFS on the basis of an MRI before any surgical treatment, at which time the tumoral burden is higher than after surgery. Here, we included patients only after GTR, based on postoperative T1 + Gd. We suppose that MT variation is subtler than before surgery and therefore we cannot reject the null hypothesis where there is no relationship between PFS/overall survival and the hMRI parameters.

Limitations of the Study

HGG is a genetically and radiologically heterogeneous disease.[59] We report a mean PFS of 52 weeks (range, 12-156 weeks), in line with current results in HGG treatment.[60] Nevertheless, considering that 75.6% of the tumors were GBMs, mean PFS is relatively good and might suggest a selection bias (inclusion of only GTRs, good KPS, for example).

The second limitation is related to a relatively small sample size.The present results cannot be generalized to all HGG, nor be used to predict individual patient outcomes.

The third limitation arises from the cross-sectional design. We acquired MP-hMRI in the postoperative phase only. Although presurgical evaluation would have been interesting, reliability overcoming postoperative brain shift during coregistration of initial and recurrence MRI scans remains a challenge.[61] The present study design compared postoperative MRIs and was thus less prone to brain shifts, although recurrence can itself result in spatial changes, and postoperative MRI artifacts can be due to blood clots, skin staples, and early postoperative vascular changes.[13] Eight weeks was considered the minimal period for postoperative modifications to disappear.

Future investigations should assess the time course of hMRI changes after initial surgery through longitudinal repeated hMRI, with the goal of determining thresholds of parameters variation suggestive of tumor infiltration.

Finally, different MR scanners were used for conventional follow-up and experimental MRI. Nevertheless, MP-hMRI is especially dedicated to be interchangeable between scanners and locations and has proven to give similar results whatever the scanner[36] (see Supplementary material). This is the first paper describing the use of hMRI in glioma patients; therefore, we acknowledge that the interval ($\Delta_{Lower} - \Delta_{Upper}$) we selected for the TOST is somewhat arbitrary. To properly define this interval, a comparison study between hMRI parameters and surgical sample histology will be carried out if the ongoing replication study confirms the importance of hMRI in recurrence prediction.

Conclusions

HGG treatment failure is partly explained by relatively imprecise radiological evaluation of brain parenchyma microinvasion. The development of new MRI biomarkers indicating brain microinvasion could lead to tailored surgical and radiation therapy treatment, with the goal of better survival and fewer neurological and cognitive side effects. This study shows a distinct pattern of MP quantitative MRI values in the area of the recurrence long before the recurrence is clinically and radiologically evident on conventional MRI. This study thus confirms that presently radiologically occult modifications occur in the cerebral microstructure while the brain is being invaded and that these modifications can be detected. If replicated on a larger scale, MP MR values could be used as MRI biomarkers of tumor progression and to target treatments.

Supplementary material

Supplementary material is available online at *Neuro-Oncology Practice* (http://nop.oxfordjournals.org/).

Acknowledgments

The authors are particularly thankful to the patients who eagerly took part in this study. We also wish to thank the Foundation Léon Frédéricq, Dr Nicolas Lambert, and the Fonds d'investissement de la recherche Scientifique du CHU de Liège.

Funding

This work was supported by the nonprofit Belgian organizations Fonds National de la Recherche Scientifique (F.R.S.-FNRS Belgium; to E.L. and C.P.), Fonds d'investissement de la recherche Scientifique du CHU de Liège, and Fondation Léon Fredericq to cover operating expenses.

Conflict of interest statement. None declared.

References

1. Korja M, Raj R, Seppä K, et al. Glioblastoma survival is improving despite increasing incidence rates: a nationwide study between 2000 and 2013 in Finland. *Neuro Oncol*. 2019;21(3):370–379.
2. Ostrom QT, Gittleman H, Stetson L, Virk SM, Barnholtz-Sloan JS. Epidemiology of gliomas. *Cancer Treat Res*. 2015;163:1–14.
3. Fyllingen EH, Hansen TI, Jakola AS, Håberg AK, Salvesen Ø, Solheim O. Does risk of brain cancer increase with intracranial volume? A population-based case control study. *Neuro Oncol*. 2018;20(9):1225–1230.
4. Raizer JJ, Fitzner KA, Jacobs DI, et al. Economics of malignant gliomas: a critical review. *J Oncol Pract*. 2015;11(1):e59–e65.
5. Sahm F, Capper D, Jeibmann A, et al. Addressing diffuse glioma as a systemic brain disease with single-cell analysis. *Arch Neurol*. 2012;69(4):523–526.

6. Watanabe M, Tanaka R, Takeda N. Magnetic resonance imaging and histopathology of cerebral gliomas. *Neuroradiology.* 1992;34(6):463–469.
7. Stummer W, Meinel T, Ewelt C, et al. Prospective cohort study of radiotherapy with concomitant and adjuvant temozolomide chemotherapy for glioblastoma patients with no or minimal residual enhancing tumor load after surgery. *J Neurooncol.* 2012;108(1):89–97.
8. Li YM, Suki D, Hess K, Sawaya R. The influence of maximum safe resection of glioblastoma on survival in 1229 patients: can we do better than gross-total resection? *J Neurosurg.* 2016;124(4):977–988.
9. Willems PWA, Taphoorn MJB, Burger H, Berkelbach van der Sprenkel JW, Tulleken CAF. Effectiveness of neuronavigation in resecting solitary intracerebral contrast-enhancing tumors: a randomized controlled trial. *J Neurosurg.* 2006;104(3):360–368.
10. Stummer W, Pichlmeier U, Meinel T, Wiestler OD, Zanella F, Reulen HJ; ALA-Glioma Study Group. Fluorescence-guided surgery with 5-aminolevulinic acid for resection of malignant glioma: a randomised controlled multicentre phase III trial. *Lancet Oncol.* 2006;7(5):392–401.
11. Jermyn M, Desroches J, Mercier J, et al. Raman spectroscopy detects distant invasive brain cancer cells centimeters beyond MRI capability in humans. *Biomed Opt Express.* 2016;7(12):5129–5137.
12. Weller M, van den Bent M, Hopkins K, et al; European Association for Neuro-Oncology (EANO) Task Force on Malignant Glioma. EANO guideline for the diagnosis and treatment of anaplastic gliomas and glioblastoma. *Lancet Oncol.* 2014;15(9):e395–e403.
13. Niyazi M, Brada M, Chalmers AJ, et al. ESTRO-ACROP guideline "target delineation of glioblastomas." *Radiother Oncol.* 2016;118(1):35–42.
14. Minniti G, Amelio D, Amichetti M, et al. Patterns of failure and comparison of different target volume delineations in patients with glioblastoma treated with conformal radiotherapy plus concomitant and adjuvant temozolomide. *Radiother Oncol.* 2010;97(3):377–381.
15. Lawrence YR, Li XA, el Naqa I, et al. Radiation dose-volume effects in the brain. *Int J Radiat Oncol Biol Phys.* 2010;76(3 suppl):S20–S27.
16. Gregor A, Cull A, Traynor E, Stewart M, Lander F, Love S. Neuropsychometric evaluation of long-term survivors of adult brain tumours: relationship with tumour and treatment parameters. *Radiother Oncol.* 1996;41(1):55–59.
17. Jenkinson MD, Smith TS, Joyce KA, et al. Cerebral blood volume, genotype and chemosensitivity in oligodendroglial tumours. *Neuroradiology.* 2006;48(10):703–713.
18. Tan WL, Xiong J, Huang WY, Wu JS, Zhan SH, Geng DY. Noninvasively detecting isocitrate dehydrogenase 1 gene status in astrocytoma by dynamic susceptibility contrast MRI. *J Magn Reson Imaging.* 2017;45(2):492–499.
19. Han Y, Yan LF, Wang XB, et al. Structural and advanced imaging in predicting MGMT promoter methylation of primary glioblastoma: a region of interest based analysis. *BMC Cancer.* 2018;18(1):215.
20. Brown R, Zlatescu M, Sijben A, et al. The use of magnetic resonance imaging to noninvasively detect genetic signatures in oligodendroglioma. *Clin Cancer Res.* 2008;14(8):2357–2362.
21. Pope WB, Prins RM, Albert Thomas M, et al. Non-invasive detection of 2-hydroxyglutarate and other metabolites in *IDH1* mutant glioma patients using magnetic resonance spectroscopy. *J Neurooncol.* 2012;107(1):197–205.
22. Ellingson BM, Gerstner ER, Smits M, et al. Diffusion MRI phenotypes predict overall survival benefit from anti-VEGF monotherapy in recurrent glioblastoma: converging evidence from phase II trials. *Clin Cancer Res.* 2017;23(19):5745–5756.
23. Regnery S, Adeberg S, Dreher C, et al. Chemical exchange saturation transfer MRI serves as predictor of early progression in glioblastoma patients. *Oncotarget.* 2018;9(47):28772–28783.
24. Cordova JS, Shu HK, Liang Z, et al. Whole-brain spectroscopic MRI biomarkers identify infiltrating margins in glioblastoma patients. *Neuro Oncol.* 2016;18(8):1180–1189.
25. Price SJ, Jena R, Burnet NG, Carpenter TA, Pickard JD, Gillard JH. Predicting patterns of glioma recurrence using diffusion tensor imaging. *Eur Radiol.* 2007;17(7):1675–1684.
26. Edwards LJ, Kirilina E, Mohammadi S, Weiskopf N. Microstructural imaging of human neocortex in vivo. *Neuroimage.* 2018;182:184–206.
27. Weiskopf N, Mohammadi S, Lutti A, Callaghan MF. Advances in MRI-based computational neuroanatomy: from morphometry to in-vivo histology. *Curr Opin Neurol.* 2015;28(4):313–322.
28. Seif M, Leutritz T, Samson R, et al. A multi-center study on fast full-brain quantitative multi-parameter mapping of R1, MT, and R2*: scan-rescan repeatability and inter-site reproducibility. Paper presented at: Joint Annual Meeting ISMRM-ESMRMB; June 16–21, 2018, Paris, France. Volume 27.
29. Callaghan MF, Freund P, Draganski B, et al. Widespread age-related differences in the human brain microstructure revealed by quantitative magnetic resonance imaging. *Neurobiol Aging.* 2014;35(8):1862–1872.
30. Freund P, Weiskopf N, Ashburner J, et al. MRI investigation of the sensorimotor cortex and the corticospinal tract after acute spinal cord injury: a prospective longitudinal study. *Lancet Neurol.* 2013;12(9):873–881.
31. Lommers E, Simon J, Reuter G, et al. Multiparameter MRI quantification of microstructural tissue alterations in multiple sclerosis. *Neuroimage Clin.* 2019;23:101879.
32. Deppe M, Duning T, Mohammadi S, et al. Diffusion-tensor imaging at 3 T: detection of white matter alterations in neurological patients on the basis of normal values. *Invest Radiol.* 2007;42(6):338–345.
33. Belhawi SM, Hoefnagels FWA, Baaijen JC, et al. Early postoperative MRI overestimates residual tumour after resection of gliomas with no or minimal enhancement. *Eur Radiol.* 2011;21(7):1526–1534.
34. Draganski B, Ashburner J, Hutton C, et al. Regional specificity of MRI contrast parameter changes in normal ageing revealed by voxel-based quantification (VBQ). *Neuroimage.* 2011;55(4):1423–1434.
35. Weiskopf N, Suckling J, Williams G, et al. Quantitative multi-parameter mapping of R1, PD(*), MT, and R2(*) at 3T: a multi-center validation. *Front Neurosci.* 2013;7:95.
36. Tabelow K, Balteau E, Ashburner J, et al. hMRI—a toolbox for quantitative MRI in neuroscience and clinical research. *Neuroimage.* 2019;194:191–210.
37. Weiskopf N, Callaghan MF, Josephs O, Lutti A, Mohammadi S. Estimating the apparent transverse relaxation time (R2*) from images with different contrasts (ESTATICS) reduces motion artifacts. *Front Neurosci.* 2014;8:278.
38. Balteau E, Leutritz T, Weiskopf N, et al. Evaluating T2* bias impact and correction strategies in quantitative proton density mapping. Paper presented at: Joint Annual Meeting ISMRM-ESMRMB; June 16–21, 2018, Paris, France.
39. Preibisch C, Deichmann R. Influence of RF spoiling on the stability and accuracy of T1 mapping based on spoiled FLASH with varying flip angles. *Magn Reson Med.* 2009;61(1):125–135.
40. Lutti A, Stadler J, Josephs O, et al. Robust and fast whole brain mapping of the RF transmit field B1 at 7T. *PLoS One.* 2012;7(3):e32379.
41. Helms G, Dathe H, Dechent P. Modeling the influence of TR and excitation flip angle on the magnetization transfer ratio (MTR) in human brain obtained from 3D spoiled gradient echo MRI. *Magn Reson Med.* 2010;64(1):177–185.
42. Collignon AM, Maes F, Delaere D, et al. Automated multi-modality image registration based on information theory. Paper presented at: XIVth International Conference on Information Processing in Medical Imaging–IPMI'95; June 26–30, 1995; Ile de Berder, France.
43. Parvez K, Parvez A, Zadeh G. The diagnosis and treatment of pseudoprogression, radiation necrosis and brain tumor recurrence. *Int J Mol Sci.* 2014;15(7):11832–11846.

44. Berndt M, Lange N, Ryang YM, et al. Value of diffusion-weighted imaging in the diagnosis of postoperative intracranial infections. *World Neurosurg.* 2018;118:e245–e253.
45. Gempt J, Förschler A, Buchmann N, et al. Postoperative ischemic changes following resection of newly diagnosed and recurrent gliomas and their clinical relevance. *J Neurosurg.* 2013;118(4): 801–808.
46. Abbasi AW, Westerlaan HE, Holtman GA, Aden KM, van Laar PJ, van der Hoorn A. Incidence of tumour progression and pseudoprogression in high-grade gliomas: a systematic review and meta-analysis. *Clin Neuroradiol.* 2018;28(3):401–411.
47. Weller M, van den Bent M, Tonn JC, et al; European Association for Neuro-Oncology (EANO) Task Force on Gliomas. European Association for Neuro-Oncology (EANO) guideline on the diagnosis and treatment of adult astrocytic and oligodendroglial gliomas. *Lancet Oncol.* 2017;18(6):e315–e329.
48. Hong JB, Roh TH, Ahn SS, et al. Predicting survival using the 2016 World Health Organization classification for anaplastic glioma. *Clin Neuropathol.* 2020;39(4):188–195.
49. Zur I, Tzuk-Shina T, Guriel M, Eran A, Kaidar-Person O. Survival impact of the time gap between surgery and chemo-radiotherapy in glioblastoma patients. *Sci Rep.* 2020;10(1):9595.
50. Blystad I, Warntjes JBM, Smedby Ö, Lundberg P, Larsson EM, Tisell A. Quantitative MRI for analysis of peritumoral edema in malignant gliomas. *PLoS One.* 2017;12(5):e0177135.
51. Lescher S, Jurcoane A, Veit A, Bähr O, Deichmann R, Hattingen E. Quantitative T1 and T2 mapping in recurrent glioblastomas under bevacizumab: earlier detection of tumor progression compared to conventional MRI. *Neuroradiology.* 2015;57(1):11–20.
52. Mehrabian H, Lam WW, Myrehaug S, Sahgal A, Stanisz GJ. Glioblastoma (GBM) effects on quantitative MRI of contralateral normal appearing white matter. *J Neurooncol.* 2018;139(1):97–106.
53. Schmierer K, Scaravilli F, Altmann DR, Barker GJ, Miller DH. Magnetization transfer ratio and myelin in postmortem multiple sclerosis brain. *Ann Neurol.* 2004;56(3):407–415.
54. Schmierer K, Tozer DJ, Scaravilli F, et al. Quantitative magnetization transfer imaging in postmortem multiple sclerosis brain. *J Magn Reson Imaging.* 2007;26(1):41–51.
55. Stüber C, Morawski M, Schäfer A, et al. Myelin and iron concentration in the human brain: a quantitative study of MRI contrast. *Neuroimage.* 2014;93(pt 1):95–106.
56. Behr SC, Villanueva-Meyer JE, Li Y, et al. Targeting iron metabolism in high-grade glioma with ^{68}Ga-citrate PET/MR. *JCI Insight.* 2018;3(21):e93999.
57. Lutti A, Dick F, Sereno MI, Weiskopf N. Using high-resolution quantitative mapping of R1 as an index of cortical myelination. *Neuroimage.* 2014;93(pt 2):176–188.
58. Bagnato F, Hametner S, Boyd E, et al. Untangling the R2* contrast in multiple sclerosis: a combined MRI-histology study at 7.0 Tesla. *PLoS One.* 2018;13(3):e0193839.
59. Chow D, Chang P, Weinberg BD, Bota DA, Grinband J, Filippi CG. Imaging genetic heterogeneity in glioblastoma and other glial tumors: review of current methods and future directions. *AJR Am J Roentgenol.* 2018;210(1):30–38.
60. Taal W, Bromberg JE, van den Bent MJ. Chemotherapy in glioma. *CNS Oncol.* 2015;4(3):179–192.
61. Gerard IJ, Kersten-Oertel M, Petrecca K, Sirhan D, Hall JA, Collins DL. Brain shift in neuronavigation of brain tumors: a review. *Med Image Anal.* 2017;35:403–420.